Towards the Analogy of Electrostatic and Electromagnetic Transducers

Richard Schroedter * **Ernst Csencsics** * **Georg Schitter** *

* *Automation and Control Institute, Technical University of Vienna, 1040 Vienna, Austria (e-mail: schroedter, csencsics, schitter @acin.tuwien.ac.at).*

Abstract: Electromechanical, or mechatronic, transducers exchange energy between the mechanical and electrical domain via electrostatic and electromagnetic transduction principles, which are the basis for actuators and sensors. This paper reveals the simple analogy between electrostatic and electromagnetic transducers. Summarizing the well-known Gauß, Ampère's, Ohm's, Chua's, Newton's, Hook's and the damping laws into a signal-flow diagram with linearized coefficients, the model shows the transducers reciprocity and physical behavior of damped spring-mass mechatronic systems. The presented modeling approach simplifies the derivation of transfer functions, the pull-in phenomenon, and the coupling factors for the design of feedback methods for mechatronic systems. The analogies are shown by comparing an electrostatic and an electromagnetic parallel-plate actuator, represented by a torsional MEMS scanning mirror and a hybrid reluctance fast steering mirror, respectively. The paper discusses the actuators performance and compares the transducer coefficients and the intrinsic stiffness regarding pull-in.

Keywords: Generic Mechatronic Transducer Model, Electromechanical Analogy, Torsional Parallel-Plate Actuator

1. INTRODUCTION

Electromechanical (also named mechatronic) transducers are fundamentally based on quasistatic magnetic and electric fields and widely applied for actuators and sensors in mechatronics, automation and control. Electromechanical systems transduce energy between stator and anchor through a working gap wherein the electromagnetic field propagates like e.g. motors. For the micro scale Lyshevski (2005) compares the energy densities in the working gap for electrostatic and electromagnetic transducers, regarding the question of which transduction principle is more powerful. Since the electrostatic field is bounded by the disruptive field strength of $E < 3$ kV/mm (Giao and Jordan (1968)) in the air gap and the electromagnetic field is bounded by the flux density saturation $B < 2.4$ T (Major and Orrock (1988)) of the ferromagnetic material, he concludes, that the electromagnetic energy density is three orders of magnitude superior compared to the electrostatic.

For applications, like satellite telecommunication mirrors (Bayat, 2011, Tab. 2-1), fast steering mirrors (Csencsics, 2017, Fig. 6.18) and scanning MEMS mirrors (Kimme et al. (2013); Holmström et al. (2014)), the achievable performance is compared for common actuation principles, which are electrostatic, piezoelectric, electromagnetic (variable reluctance) and electrodynamic (moving coil) transducers. Tilmans (1996) points out inherent analogies and proposes an equivalent electric circuit to describe electromechanical systems with lumped parameters. Further systematization of the transducer principle is presented by Preumont (2006) and Janschek (2012) introducing a generic mechatronic system model. The extension of this model can, however, provide a clear depiction of the electromagnetic and mechanical field duality with the transducers in between and help to design actuators and sensors that overcome current limitations. In particular, the analogies of transducer coefficients and stiffening of electrostatic and electromagnetic torsional parallel-plate systems are rarely discussed in literature so far.

The contribution of this paper is a generic mechatronic modeling approach for electrostatic and electromagnetic systems based on a signal-flow block diagram with linearized coefficients, which reveals symmetries and analogies of both transduction principles. The signal-flow diagram is an extension of the generic mechatronic system model with lumped parameters from Janschek (2012). It clearly shows the duality of energy and power variables as well as storages and dissipators, and provides a complete model for the electrical and mechanical domain. For the sake of completeness, Chua's memristor (Chua (1971)) is added as a damping element in the electrical and mechanical domain. This generic mechatronic modeling approach is discussed along two examples of electrostatic and electromagnetic torsional parallel-plate actuators: an electrostatic torsional micro-electro-mechanical system (MEMS) scanning mirror (Kiessling et al. (2004)) and a hybrid reluctance fast steering mirror (FSM) (Csencsics et al. (2018)). Finally, the nonlinear behavior and pull-in instability (negative differential system stiffness) are discussed, that affect the actuator range and performance.

* This work has been supported in part by the Austrian Research Promotion Agency (FFG).

Post-print version of the article: Richard Schroedter, Ernst Csencsics, Georg Schitter, "Towards the Analogy of Electrostatic and Electromagnetic Transducers", *Proc. of the 21th IFAC World Congress, Virtual Conference, Berlin, July 11-17*, 2020.

For further information contact: schroedter@acin.tuwien.ac.at, https://orcid.org/0000-0003-3259-4571

2. GENERIC MECHATRONIC TRANSDUCER

The generic mechatronic transducer model describes the working principles of sensors and actuators that transform energy between mechanic and electric variables, while the transducer itself does not dissipate energy (Janschek (2012)). Transducers can be used as sensor as well as actuator, and even at the same time when using 'self-sensing' methods. The generic mechatronic transducer is illustrated in Fig. 1 as a two-port network.

Fig. 1. Generic mechatronic transducer by Janschek (2012).

2.1 Physical laws

There are four basic variables for the electrical as well as the mechanical domain. In the electrical domain these are the energy variables *charge* q and *flux linkage* ψ and the power variables *current* i and *voltage* v. In the mechanical domain these are the energy variables *position* x and *momentum* p and the power variables *velocity* $\dot{x}$ and *force* F. Herein, the power variables are defined by time the derivative of the corresponding energy variable according to the fundamental physical laws for

$$\text{Electric current:} \quad i = \frac{\mathrm{d}\,q}{\mathrm{d}t} = \dot{q}, \tag{1a}$$

$$\text{Faraday's law (induction):} \quad v = \frac{\mathrm{d}\,\psi}{\mathrm{d}t} = \dot{\psi}, \tag{1b}$$

$$\text{Force:} \quad F = \frac{\mathrm{d}\,p}{\mathrm{d}t} = \dot{p}, \tag{1c}$$

$$\text{Velocity:} \quad \dot{x} = \frac{\mathrm{d}\,x}{\mathrm{d}t}. \tag{1d}$$

The energy storages are *capacitance* C and *inductance* L in the electrical domain as well as *stiffness* k and *mass* m in the mechanical domain. Between energies and power variables dissipators are defined by the *resistor* R and the *memristor* M (Chua (1971)) in the electrical domain, and the *damper* d and the *memdamper* B (Jeltsema and van der Schaft (2010); Fouda et al. (2015)) in the mechanical domain. Both memory dissipators are an extension to the model from Janschek (2012). The memristive element was quite recently obtained and constructed by Strukov et al. (2008) as well as the concept of a memdamper or tapered dashpot e.g. Jeltsema and van der Schaft (2010) and could be applied for passive damping in dynamic systems. The corresponding linearized material equations are

$$\text{Gauß's law:} \quad q = C \cdot v \tag{2a}$$

$$\text{Ampère's law:} \quad \psi = L \cdot i \tag{2b}$$

$$\text{Ohm's law:} \quad v = R \cdot i \tag{2c}$$

$$\text{Chua's law:} \quad \psi = M \cdot q \tag{2d}$$

$$\text{Newton's law:} \quad p = m \cdot \dot{x} \tag{2e}$$

$$\text{Hook's law:} \quad F = k \cdot x \tag{2f}$$

$$\text{Damping:} \quad F = d \cdot \dot{x} \tag{2g}$$

$$\text{Memdamping:} \quad p = B \cdot x \tag{2h}$$

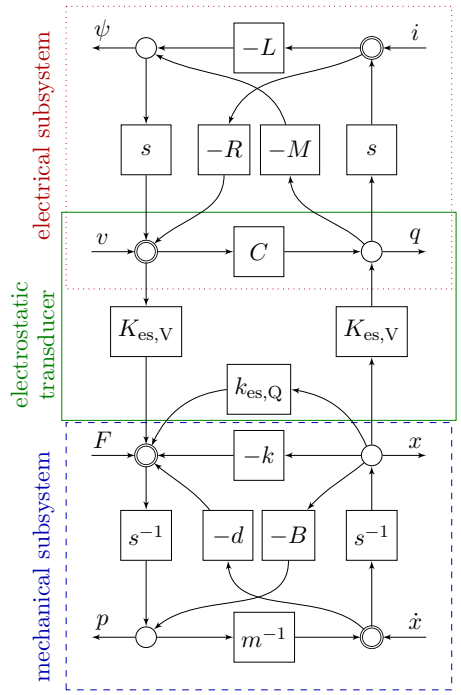

(a) electrostatic

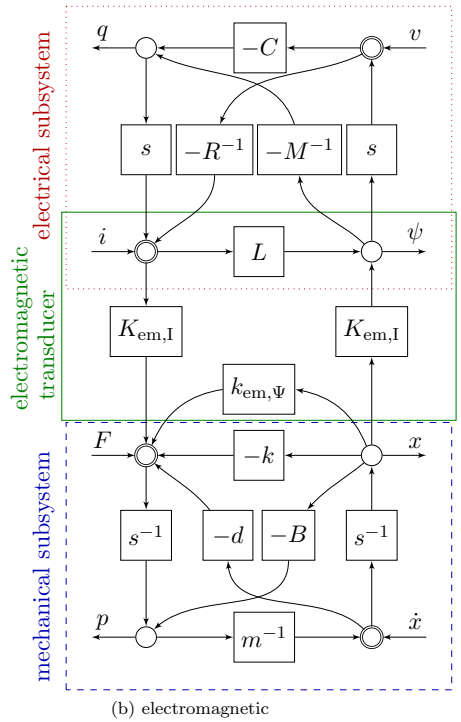

(b) electromagnetic

Fig. 2. Signal-flow diagram of generic linear mechatronic systems: (a) *voltage* driven *electrostatic* system and (b) *current* driven *electromagnetic* system.

Post-print version of the article: Richard Schroedter, Ernst Csencsics, Georg Schitter, "Towards the Analogy of Electrostatic and Electromagnetic Transducers", *Proc. of the 21th IFAC World Congress, Virtual Conference, Berlin, July 11-17*, 2020.

For further information contact: schroedter@acin.tuwien.ac.at, https://orcid.org/0000-0003-3259-4571

2.2 Signal-flow diagram

Figure 2 illustrates the signal-flow diagram of the generic linear transducer model for the electrostatic (Fig. 2a) and electromagnetic (Fig. 2b) mechatronic system with lumped parameters linearized around an operation point. The part in the green box describes the electrostatic and electromagnetic transducers, coupling energy between the upper electrical and lower mechanical system. Note, that the relations (1) and (2) are represented in the signal-flow diagrams. The *energy variables* are illustrated with single-bordered circles ○, while *power variables* have double-bordered circles ◎. Both symbols represent a sum. Shown with power drives the electrostatic transducer is driven with a voltage and the electromagnetic transducer is driven with a current. The signal-flow diagram in Fig. 2 is arranged symmetrically, with the storage elements (L, C, $k_{\mathrm{es,Q}}$, $k_{\mathrm{em},\Psi}$, k, m) on the vertical middle axis between power and energy variables. The Laplace variable s is used when going from a power to an energy variable, while s^{-1} is used in the vice versa case. The dampers are placed in the center of the mechanical (d, B) or electrical (R, M) two-port systems connecting either power or energy variables. The transducer coefficients or motor constants (K_{es}, K_{em}) only transduce either power or energy, while within the mechatronic transducer itself no dissipation occurs. The transducer stiffness and coefficient, linearized from the forces $F_{\mathrm{es}} = \frac{1}{2}\frac{\partial C(x)}{\partial x} v^2$ and $F_{\mathrm{em}} = \frac{1}{2}\frac{\partial L(x)}{\partial x} i^2$, are for the electrostatic voltage drive

$$K_{\mathrm{es,V}} = \frac{\partial C(x)}{\partial x} v\Big|_{\substack{v=v_0\\x=x_0}}, \quad k_{\mathrm{es,V}} = \frac{1}{2}\frac{\partial^2 C(x)}{\partial x^2} v^2\Big|_{\substack{v=v_0\\x=x_0}}, \tag{3a}$$

$$C = C(x)\big|_{x=x_0}, \tag{3b}$$

and for electromagnetic current drive

$$K_{\mathrm{em,I}} = \frac{\partial L(x)}{\partial x} i\Big|_{\substack{i=i_0\\x=x_0}}, \quad k_{\mathrm{em,I}} = \frac{1}{2}\frac{\partial^2 L(x)}{\partial x^2} i^2\Big|_{\substack{i=i_0\\x=x_0}}, \tag{4a}$$

$$L = L(x)\big|_{x=x_0}. \tag{4b}$$

The capacitance C and inductance L are considered as part of the mechatronic transducer and the transducer stiffnesses shown in Fig. 2 are defined as (Janschek (2012))

$$k_{\mathrm{es,V}} = k_{\mathrm{es,Q}} + \frac{K_{\mathrm{es,V}}^2}{C}, \quad k_{\mathrm{em,I}} = k_{\mathrm{em},\Psi} + \frac{K_{\mathrm{em,I}}^2}{L}, \tag{5}$$

where the indices V, Q, I, Ψ denote the cases for voltage, charge, current or flux drive.

2.3 Transfer function

The transfer functions from input to output can be derived directly from Fig. 2, where common rules for signal-flow diagrams from control theory are applied. For example the transfer function $G_{x/v}$ with $L = 0$, $R = M = 0$ is derived from x to v considering the arrow direction in Fig. 2a. If the arrow points towards the destination variable (e. g. x) a positive, and otherwise a negative sign is considered. First, all equations with x are noted as

$$\dot{x} = s\,x, \qquad F = -(k_{\mathrm{es,Q}} - k)\,x, \tag{6a}$$

$$q = -K_{\mathrm{es,V}}\,x, \qquad p = -(-B)\,x. \tag{6b}$$

Then, all equations from the newly obtained variables $\dot{x}$, F and q are noted as

$$p = m\,\dot{x}, \qquad F = -(-d)\,\dot{x}, \tag{7a}$$

$$v = K_{\mathrm{es,V}}^{-1}\,F, \qquad p = s^{-1}\,F, \qquad v = C^{-1}\,q. \tag{7b}$$

Now, all equations (6) and (7) are inserted and added according to the summations in Fig. 2, so that only the variables x and v remain

$$\begin{aligned} v =& K_{\mathrm{es,V}}^{-1}\left((k - k_{\mathrm{es,Q}})\,x + s\,d\,x + s\,B\,x + m\,s^2\,x\right)\ldots \\ &\ldots - C^{-1}\,K_{\mathrm{es,V}}\,x \end{aligned} \tag{8}$$

Finally, the desired transfer function $G_{x/v}$ with (5) is

$$G_{\mathrm{x/v}} = \frac{x}{v} = \frac{K_{\mathrm{es,V}}}{m\,s^2 + (d + B)\,s + k - k_{\mathrm{es,V}}}. \tag{9}$$

2.4 Pull-In phenomenon and coupling factor

According to Kirchhoff's mesh equation from x to F considering the mechanical system (cf. Fig. 2), the resonance frequencies are found to be

$$\Omega_{\mathrm{es,V}}^2 = \frac{k - k_{\mathrm{es,V}}}{m}, \qquad \omega_{\mathrm{es,Q}}^2 = \frac{k - k_{\mathrm{es,Q}}}{m}, \tag{10a}$$

$$\Omega_{\mathrm{em,I}}^2 = \frac{k - k_{\mathrm{em,I}}}{m}, \qquad \omega_{\mathrm{em},\Psi}^2 = \frac{k - k_{\mathrm{em},\Psi}}{m}. \tag{10b}$$

In general, pull-in occurs, when the differential system stiffness becomes negative, $\partial F_{\Sigma}/\partial x < 0$, including all forces at the node F. Figure 2 reveals inner loops, that may cause static pull-in instability, when the transducer stiffness becomes greater than the mechanical stiffness k

$$k_{\mathrm{es,Q}} + \frac{K_{\mathrm{es,V}}^2}{C} - k = k_{\mathrm{es,V}} - k \geq 0, \tag{11a}$$

$$k_{\mathrm{em},\Psi} + \frac{K_{\mathrm{em,I}}^2}{L} - k = k_{\mathrm{em,I}} - k \geq 0. \tag{11b}$$

It is noteworthy, that the pull-in occurs for the electromechanical coupling factor $\kappa^2 = 1$, which are defined by (Janschek (2012))

$$\kappa_{\mathrm{es}}^2 = \frac{\omega_{\mathrm{es,Q}}^2 - \Omega_{\mathrm{es,V}}^2}{\omega_{\mathrm{es,Q}}^2} = \frac{k_{\mathrm{es,V}} - k_{\mathrm{es,Q}}}{k - k_{\mathrm{es,Q}}} = \frac{K_{\mathrm{es,V}}^2}{C}\frac{1}{k - k_{\mathrm{es,Q}}}, \tag{12a}$$

$$\kappa_{\mathrm{em}}^2 = \frac{\omega_{\mathrm{em},\Psi}^2 - \Omega_{\mathrm{em,I}}^2}{\omega_{\mathrm{em},\Psi}^2} = \frac{k_{\mathrm{em,I}} - k_{\mathrm{em},\Psi}}{k - k_{\mathrm{em},\Psi}} = \frac{K_{\mathrm{em,I}}^2}{L}\frac{1}{k - k_{\mathrm{em},\Psi}}. \tag{12b}$$

3. EXAMPLES: TORSIONAL PARALLEL-PLATE ACTUATORS

To demonstrate the validity of the mechatronic system model and reveal analogies, it is applied to torsional parallel-plate actuators with the basic configuration shown in Fig. 3 from each transducer domain, electrostatic and electromagnetic.

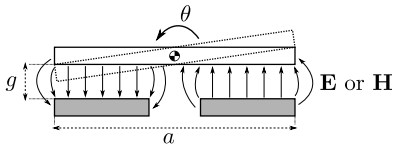

Fig. 3. Basic principle of parallel plate configuration actuators with field lines of electric field $\boldsymbol{E}$ or magnetic field $\boldsymbol{H}$ and torsion θ.

Post-print version of the article: Richard Schroedter, Ernst Csencsics, Georg Schitter, "Towards the Analogy of Electrostatic and Electromagnetic Transducers", *Proc. of the 21th IFAC World Congress, Virtual Conference, Berlin, July 11-17*, 2020.

For further information contact: schroedter@acin.tuwien.ac.at, https://orcid.org/0000-0003-3259-4571

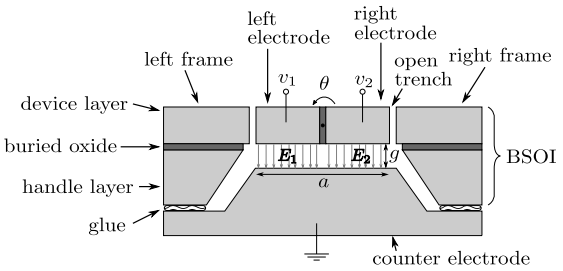

Fig. 4. Electrostatic parallel-plate MEMS mirror, adapted from Kiessling (2007).

3.1 Electrostatic torsional parallel-plate actuator

Figure 4 shows the cross section of the parallel-plate MEMS scanning mirror from Kiessling (2007). The mirror plate, the upper part of a bonded silicon of insulator wafer (BSOI), is split into two potentials (left and right electrode), which are isolated with filled oxide trenches. The counter electrode is a second wafer, which is glued on the bottom of the first wafer. Two different voltages towards the counter electrode lead to a deflection of the mirror plate. The electrostatic torque is (Kiessling (2007))

$$\tau_{\text{es}} = \frac{1}{2}\frac{\partial C(\theta)}{\partial \theta} v^2 = \frac{1}{2} v^2 \int_0^{a/2} \frac{\varepsilon\, b\, x\, \mathrm{d}x}{(g - x \cdot \tan\theta)^2}, \tag{13}$$

where a and b are the mirror plate width and length, g the initial gap distance and ε the permittivity of the material in the gap. The capacitance derivative can be denoted as

$$\frac{\partial C(\gamma)}{\partial \gamma} = \frac{\varepsilon b a^2}{4 g^2 \gamma^2}\left[\frac{\gamma}{1-\gamma} + \ln(1-\gamma)\right], \tag{14}$$

with the normalized deflection γ (Sattler et al. (2002))

$$\gamma = \frac{\tan(\theta)}{\tan(\theta_{\max})} = \frac{a\tan(\theta)}{2g}, \quad \tan(\theta_{\max}) = \frac{2g}{a}. \tag{15}$$

Then, the integral and the second derivative are

$$C(\gamma) = \frac{\varepsilon b a}{2g\gamma}\ln(1-\gamma), \tag{16}$$

$$\frac{\partial^2 C(\gamma)}{\partial \gamma^2} = \frac{\varepsilon b a^3}{8 g^3 \gamma^3}\left[\frac{\gamma^2}{(1-\gamma)^2} - 2\ln(1-\gamma) - \frac{2\gamma}{1-\gamma}\right]. \tag{17}$$

With $k_{\text{es,V}} - k = 0$ from (11) or $\kappa_{\text{es}}^2 = 1$, the pull-in for a linear spring torque $k\,\theta = \tau_{\text{es}}$ is derived to be at $\gamma_{\text{PI}} = 0.4404$ by solving $\gamma \cdot \frac{\partial^2 C(\gamma)}{\partial \gamma^2} - \frac{\partial C(\gamma)}{\partial \gamma} \equiv 0$ with (14) and (17) (cf. Nemirovsky and Bochobza-Degani (2001)). The pull-in voltage with (11) and (17) results in

$$v_{\text{PI,V}} = \sqrt{2k\left(\frac{\partial^2 C(\gamma_{\text{PI}})}{\partial \gamma^2}\right)^{-1}} = \sqrt{\frac{6.6196\, k\, g^3}{\varepsilon\, b\, a^3}}. \tag{18}$$

The electrostatic transducer coefficient and stiffness (3) linearized at zero deflection ($\gamma = 0$) are

$$K_{\text{es,V},0} = \varepsilon\frac{a^2 b}{8g^2} v_0, \qquad k_{\text{es,V},0} = \varepsilon\frac{a^3 b}{24 g^3} v_0^2. \tag{19}$$

For the silicon MEMS mirror example from Kiessling (2007) with a plate size of a = b = 1 mm, g = 100 µm gap, $k = 0.23$ µNm/rad stiffness and 1 kHz eigenfrequency, the pull-in voltage (18) is $v_{\max} = 415$ V at the angle $\theta_{\max} = 5\,°$. Hence with $v_0 = v_{\max}$ the transducer coefficients (19) are $K_{\text{es,V},0} = 46$ pNm/V and $k_{\text{es,V},0} = 64$ nNm/rad.

Kiessling (2007) shows, that the MEMS mirror behaves according to (9) like a second order oscillation system

$$G_{\theta/\text{v}} = \frac{\theta}{v} = \frac{K_{\text{es,V}}}{J\,s^2 + d\,s + k - k_{\text{es,V}}}. \tag{20}$$

3.2 Electromagnetic parallel-plate actuator

In Fig. 5 the cross section of one system axis of a parallel plate hybrid reluctance actuated fast steering mirror is depicted, cf. Csencsics et al. (2018). The actuator consists

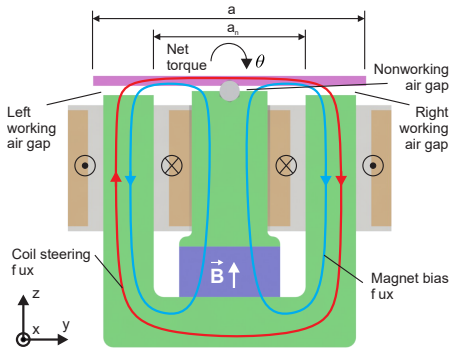

Fig. 5. Electromagnetic torsional parallel plate actuator Csencsics et al. (2018).

of a permanent magnet (blue), generating a biasing flux (blue line), which passes through the non-working and the working air gaps and is guided by the ferromagnetic mover (magenta) and yoke parts (green). With the mover in the middle position and zero current, there is no net torque on the mover as the biasing flux is equally distributed over the right and left air gap. A current through the actuator coils generates a magnetic steering flux (red line), passing only through the outer yoke part and the mover due to the high reluctance the permanent magnet represents to an outer field. The steering and biasing flux are superimposed in the working air gaps, yielding an increased flux in the right air gap and a clockwise net torque on the mover. Due to the permanent magnet the actuator has a negative stiffness, which makes the system open-loop unstable but can be compensated by a mechanical flexure, suspending the mover. The second axis of the systems is arranged perpendicular to the first one, forming one magnetic circuit with the first axis. The total force that acts on an electromagnetic actuator, including the reluctance force, is obtained from Munnig Schmidt et al. (2014) as

$$F_{\text{em}} = N\,I\,\frac{\partial \Psi_w}{\partial x} - \frac{1}{2}\frac{\partial L(x)}{\partial x} i^2. \tag{21}$$

The first term represents the linear relation of force to current, present in any electromagnetic actuator, while the second term with the squared relation of force to current is caused by the magnetic energy stored in the self-inductance. In the case of the hybrid reluctance actuator the self-inductance of the coils is hardly influenced by the position of the mover, as the reluctance of the coils is determined by the reluctance of the two working air gaps in series. As one gap gets bigger the other gets smaller, such that the second term in (21) can be neglected.

Post-print version of the article: Richard Schroedter, Ernst Csencsics, Georg Schitter, "Towards the Analogy of Electrostatic and Electromagnetic Transducers", *Proc. of the 21th IFAC World Congress, Virtual Conference, Berlin, July 11-17*, 2020.

For further information contact: schroedter@acin.tuwien.ac.at, https://orcid.org/0000-0003-3259-4571

Via the Maxwell stress tensor the resulting torque can be calculated, see Wu et al. (2010), and results to

$$\tau_{\text{em}} = \frac{\Psi_r^2 - \Psi_l^2}{2\mu A} \cdot \frac{a}{2} = \tau_{\text{em}} = K_{\text{em,I}} \cdot i + k_{\text{em,I}} \cdot \theta \quad (22)$$

with Ψ_r and Ψ_l the magnetic flux in the right a left air gap, A the cross section of the air gaps, a the full plate width (and $a/2$ the force lever arm), the motor constant $K_{\text{em,I}}$ and the actuator stiffness $k_{\text{em,I}}$. The y dependent local length of the working air gap for a plate tilted by θ is defined by $g - y\tan(\theta)$ (cf. Ito et al. (2019)), with g the length of the working air gaps with the plate in the middle position. Integrating y from $\beta \cdot a/2$ to $a/2$, with $\beta = a_n/a$ obtained from the nonworking and entire width of the plate (y-direction in Fig. 5), and using the normalized angle γ from (15), the motor constant and actuator stiffness are

$$K_{\text{em,I}}(\gamma) = \frac{\mu A N \lambda H_c l_m a \chi \left(\operatorname{artanh}(\chi\gamma) - \operatorname{artanh}(\beta\chi\gamma)\right)}{2g^2\gamma}, \quad (23)$$

$$k_{\text{em,I}}(\gamma) = \frac{\mu A \lambda^2 H_c^2 l_m^2 \chi^4 (a^2 + 4g^2\gamma^2)(1-\beta^2)}{4g^3} \cdots$$

$$\cdots \times \frac{(1 + \chi^2\gamma^2 + \beta^2\chi^2\gamma^2 - 3\beta^2\chi^4\gamma^4)}{(1-\chi^2\gamma^2)^2\,(1-\beta^2\chi^2\gamma^2)^2}, \quad (24)$$

$$\text{with} \quad \chi = \sqrt{g/(g + 2l_m + 2l_n)}, \quad (25)$$

where are N the sum of turns of both coils, λ a factor to consider the flux leakage, H_c the coercivity and l_m the length of the permanent magnet, a the full plate width, l_n the length of the non-working air gap. The linearized coefficients at zero deflection ($\gamma = 0$) are

$$K_{\text{em,I,0}} = \frac{\mu A N \lambda H_c l_m a (1-\beta)}{2\,g\,(g + 2l_m + 2l_n)}, \quad (26)$$

$$k_{\text{em,I,0}} = \frac{\mu A \lambda^2 H_c^2 l_m^2 a^2 (1-\beta^2)}{4\,g\,(g + 2l_m + 2l_n)^2}, \quad (27)$$

resulting to $K_{\text{em,I,0}} = 0.03\,\text{Nm/A}$ and $k_{\text{em,I,0}} = 2.3\,\text{Nm/rad}$ for the design parameters of the hybrid reluctance actuated FSM (Csencsics (2017)). Disregarding structural modes of the mechanical structure, the resulting transfer function from current input to angular position is essentially a mass-spring-damper system

$$G_{\theta/\text{i}} = \frac{\theta}{i} = \frac{K_{\text{em,I}}}{J\,s^2 + d\,s + k - k_{\text{em,I}}} \quad (28)$$

with J the inertia of the mover, d the damping factor and k the stiffness of the mechanical flexure. The effective stiffness for the actuator for each operating point is obtained from $k - k_{\text{em,I}}$. The FSM is designed for a range of $\pm 3°$, with the dynamics showing a small signal tilting mode at around 110 Hz. With a PID-based feedback controller the system achieves a bandwidth as high as 1 kHz.

4. DISCUSSION

With (20) and (28) similar system dynamics are obtained, only differing in their transducer coefficient and stiffness. Figure 6 shows the normalized transducer coefficients. For the electrostatic MEMS mirror either the left or the right gap (E_1 or E_2 in Fig. 4) is driven with a voltage according to the direction of the deflection. Therefore, the transducer coefficient $K_{\text{es,V}}$ has no continuous derivatives at zero deflection. In contrast, the electromagnetic flux lines in the FSM from Fig. 5 go through the mirror plate and both gaps, causing a continuous derivative of $K_{\text{em,I}}$ at zero

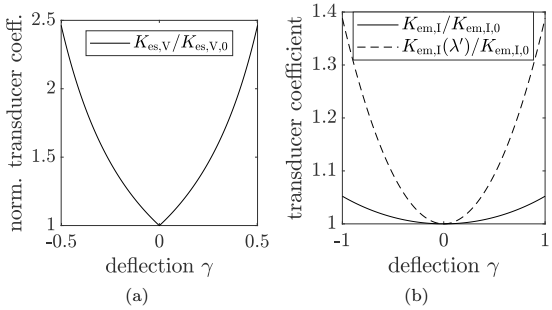

Fig. 6. Transducer coefficients: (a) electrostatic and (b) electromagnetic.

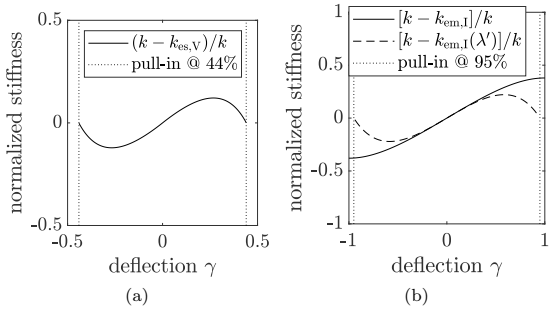

Fig. 7. Forces with transducer stiffness softening and pull-in: (a) electrostatic and (b) electromagnetic.

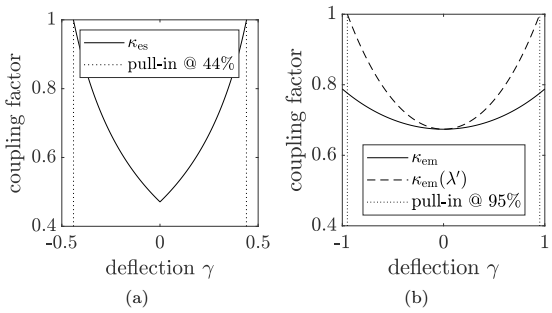

Fig. 8. Transducer coupling factor with pull-in for $\kappa = 1$: (a) electrostatic and (b) electromagnetic.

deflection. Figure 7 shows the normalized actuator stiffness of both systems. The electrostatic parallel-plate transducer has a pull-in at 44 % of the possible deflection range for voltage control (71 % for charge control, Sattler et al. (2002)), while the electromagnetic does not exhibit pull-in considering a constant flux leakage factor λ (in contrary to typical reluctance actuators Chen and Ho (2004)). In reality, the hybrid reluctance actuator features a flux leakage (Ito et al. (2019)) and the flux efficiency factor $\lambda = \lambda'(\gamma)$ is usually nonlinear. Applying the simulation results of a similar hybrid reluctance actuator from (Cigarini et al., 2019, Fig. 7) approximated as square function with

$$\lambda'(\gamma) = 0.23\,\gamma^2 + 0.72, \quad (29)$$

the pull-in of the FSM does occur at 95 % deflection, as shown in Fig. 7b. Plotting the coupling factor in Fig. 8 reveals, that pull-in for both systems happens at $\kappa = 1$.

Post-print version of the article: Richard Schroedter, Ernst Csencsics, Georg Schitter, "Towards the Analogy of Electrostatic and Electromagnetic Transducers", *Proc. of the 21th IFAC World Congress, Virtual Conference, Berlin, July 11-17*, 2020.

For further information contact: schroedter@acin.tuwien.ac.at, https://orcid.org/0000-0003-3259-4571

The comparison of the transducer coefficients normalized to the inertia and maximum drive amplitude $K_{\mathrm{es,V},0} \cdot v_{\max}/J = 187 \cdot 10^6\,^\circ/\mathrm{s}^2$ and $K_{\mathrm{em,I},0} \cdot i_{\max}/J = 473 \cdot 10^3\,^\circ/\mathrm{s}^2$ reveals a 3 orders of magnitude larger angular acceleration for the electrostatic actuator, which is due to the small mass of the MEMS mirror of 70 µg compared to 61 g for the FSM.

Usually feedback control is required for fast trajectory tracking and stabilizing the actuator to overcome these nonlinearities and pull-in limits. For feedback of the reluctance actuator Csencsics et al. (2018) applies eddy current sensors, while for the MEMS mirror control Kiessling (2007) proposes self-sensing with additional electrostatic combs.

In summary a holistic model for a linearized mechatronic system with electromechanical transducer is developed, which makes the analogies of electrostatic and electromagnetic transducers clearly evident and is validated along the example of two torsional parallel-plate actuated mirror systems.

5. CONCLUSION

This paper proposes a novel holistic model for electromechanical, or mechatronic, systems with lumped parameters in the form of a structured signal-flow block diagram, explicitly revealing the analogies between electrostatic and electromagnetic transducer principles. Its applicability and relevance for the modeling of an arbitrary mechatronic system is demonstrated for two systems with torsional parallel-plate actuators based on an electrostatic and an electromagnetic actuation principle, respectively. With the obtained formalized transducer coefficients, stiffness and coupling factors the model provides an enhanced insight into the designed system, e. g. revealing the pull-in point, as well as the interplay between the various system components and domains. Future work is concerned with validating the holistic model for further mechatronic systems with other actuator types, including voice coil, piezoelectric and reluctance actuation, and drive modes in order to demonstrate the generality of this unified modeling framework.

REFERENCES

Bayat, D. (2011). *Large Hybrid High Precision MEMS Mirrors*. Dissertation, École Polytechnique Fédérale de Lausanne, Lausanne.

Chen, K.S. and Ho, C.C. (2004). Electromagnets calibration utilizing the pull-in instability. *Precision Engineering*, 28(1), 106–115.

Chua, L. (1971). Memristor-The missing circuit element. *IEEE Transactions on Circuit Theory*, 18(5), 507–519.

Cigarini, F., Ito, S., Troppmair, S., and Schitter, G. (2019). Comparative Finite Element Analysis of a Voice Coil Actuator and a Hybrid Reluctance Actuator. *IEEJ Journal of Industry Applications*, 8(2), 192–199.

Csencsics, E., Schlarp, J., and Schitter, G. (2018). High-Performance Hybrid-Reluctance-Force-Based Tip/Tilt System: Design, Control, and Evaluation. *IEEE/ASME Transactions on Mechatronics*, 23(5), 2494–2502.

Csencsics, E. (2017). *Integrated Design of High Performance Mechatronics for Optical Inline Metrology Systems*. Dissertation, Automation and Control Institute (ACIN), Vienna University of Technology, Austria.

Fouda, M.E., Radwan, A.G., Elwakil, A.S., and Nawayseh, N.K. (2015). Review of the missing mechanical element: Memdamper. In *IEEE International Conference on Electronics, Circuits, and Systems (ICECS)*, 201–204.

Giao, T. and Jordan, J. (1968). Modes of Corona Discharges in Air. *IEEE Transactions on Power Apparatus and Systems*, PAS-87(5), 1207–1215.

Holmström, S.T.S., Baran, U., and Urey, H. (2014). MEMS Laser Scanners: A Review. *Journal of Microelectromechanical Systems*, 23(2), 259–275.

Ito, S., Troppmair, S., Lindner, B., Cigarini, F., and Schitter, G. (2019). Long-Range Fast Nanopositioner Using Nonlinearities of Hybrid Reluctance Actuator for Energy Efficiency. *IEEE Transactions on Industrial Electronics*, 66(4), 3051–3059.

Janschek, K. (2012). *Mechatronic Systems Design - Methods, Models, Concepts*. Springer.

Jeltsema, D. and van der Schaft, A.J. (2010). Memristive port-Hamiltonian Systems. *Mathematical and Computer Modelling of Dynamical Systems*, 16(2), 75–93.

Kiessling, T. (2007). *Quasistatisch Auslenkbarer Kippspiegel Zur Ablenkung von Licht*. Dissertation, Technischen Universität Dresden, Dresden.

Kiessling, T., Wolter, A., Schenk, H., and Lakner, H. (2004). Bulk micromachined quasistatic torsional micromirror. In A. El-Fatatry (ed.), *Micromachining and Microfabrication*, 193. San Jose, CA.

Kimme, S., Sandner, T., Graf, A., and Todt, U. (2013). Actuation Principles for Hybrid Two-Dimensional Quasistatic Micro Scanning Mirrors. In *Conf. on Optical Technologies for Sensing and Measurement*, 22–27.

Lyshevski, S.E. (2005). *Nano- and Micro-Electromechanical Systems: Fundamentals of Nano- and Microengineering*. CRC Press, 2 edition.

Major, R. and Orrock, C. (1988). High saturation ternary cobalt-iron basalt alloys. *IEEE Transactions on Magnetics*, 24(2), 1856–1858.

Munnig Schmidt, R., Schitter, G., and Rankers, A. (2014). *The Design of High Performance Mechatronics: High-Tech Functionality by Multidisciplinary System Integration*. IOS Press.

Nemirovsky, Y. and Bochobza-Degani, O. (2001). A methodology and model for the pull-in parameters of electrostatic actuators. *Journal of Microelectromechanical Systems*, 10(4), 601–615.

Preumont, A. (2006). *Mechatronics: Dynamics of Electromechanical and Piezoelectric Systems*. Number 136 in Solid Mechanics and Its Applications. Springer.

Sattler, R., Plötz, F., Fattinger, G., and Wachutka, G. (2002). Modeling of an electrostatic torsional actuator: Demonstrated with an RF MEMS switch. *Sensors and Actuators A: Physical*, 97-98, 337–346.

Strukov, D.B., Snider, G.S., Stewart, D.R., and Williams, R.S. (2008). The missing memristor found. *Nature*, 453(7191), 80–83.

Tilmans, H.A.C. (1996). Equivalent circuit representation of electromechanical transducers: I. Lumped-parameter systems. *Journal of Micromechanics and Microengineering*, 6(1), 157–176.

Wu, D., Xie, X., and Zhou, S. (2010). Design of a Normal Stress Electromagnetic Fast Linear Actuator. *IEEE Transactions on Magnetics*, 46(4), 1007–1014.

Post-print version of the article: Richard Schroedter, Ernst Csencsics, Georg Schitter, "Towards the Analogy of Electrostatic and Electromagnetic Transducers", *Proc. of the 21th IFAC World Congress, Virtual Conference, Berlin, July 11-17*, 2020.

For further information contact: schroedter@acin.tuwien.ac.at, https://orcid.org/0000-0003-3259-4571